Arabian Journal of Chemical and Environmental Research

Vol. 10 Issue 1 (2023) 35–49

Studies of the adsorption capacity of ziziphus mauritania seed shells for the adsorption of cationic and anionic dyes

A. S. Usman[1*], M. B. Ibrahim[2], B. Usman[2], Z. Hashim[2], M. M. Lawan[1]

[1]*Department of Chemistry, Faculty of Science, Yobe State University, Damaturu, Nigeria*
[2]*Department of Pure and Industrial Chemistry, Faculty of Physical Sciences, College of Natural and Pharmaceutical Sciences, Bayero University Kano, Nigeria*

Received 18 July 2023, Revised 17 June 2023, Accepted 19 June 2023

Abstract

The adsorption capacity of activated carbon prepared from seed shells of Ziziphus Mauritania was studied using Methylene blue (MB), methyl orange (MO) and Rhodamine B (RB) dyes. The adsorbent was prepared by chemical activation using Phosphoric acid then characterized by SEM and FTIR. Analysis of point of zero charge (pHPZC), Ash content, moisture content and bulk density have also been carried out. The study of the adsorption capacity of the activated carbon was carried out using the batch adsorption method. The effects of influencing parameters such as contact time, adsorbent dosage, initial dye concentration, temperature and pH were investigated. The removals of the cationic MB and RB dyes were better in basic pH while the adsorption of MO was better in acid pH. The maximum adsorption capacities for MB, MO and RB were 80.79, 99.35 and 89.15 mg/g respectively. The adsorption data have been fitted into the kinetic models and the best fit was obtained by the pseudo-second-order model. The equilibrium data revealed that the adsorption of MO obeyed the Langmuir isotherm while the removals of MB and RB obeyed the Freundlich isotherm. The thermodynamic studies revealed that all the adsorption processes were spontaneous and endothermic. Based on the foregoing findings, ZM-H3PO4 can be a potential adsorbent for the removal of cationic and anionic dyes.

Keywords: Ziziphus mauritania, Adsorption, Activated carbon, Isotherms, Adsorption Kinetics

*Corresponding author.
E-mail address: abdullerhy135@gmail.com

1. Introduction

Synthetic dyes are extensively used in a wide range of industries amongst which textile processing industries are the major consumers (Keharia *et al.*, 2003). One of the main sources of severe pollution problems worldwide is the textile industry and its dye-containing wastewater (Baban *et al.*, 2010). A significant amount of the textile dyes are directly discharged as aqueous effluents in different environmental components. Many of the dyes released and their breakdown products are toxic, carcinogenic or mutagenic to life forms because they contain carcinogens, such as benzidine, naphthalene and other aromatic compounds (Suteu *et al.*, 2009). The genotoxicity of textile dyes is the greatest potential long-term hazard to human health (Christie *et al.*, 2007). Some dyes like Azure-B, Rhodamine B, Methylene blue and methyl orange which are widely used in the textile industries reveal mutagenic potentiality (Hunger *et al.*, 2003; Goscianska et al., 2015), teratogenicity, and can cause gastrointestinal complications, respiratory disorder and diseases of the central nervous system (Ramsay *et al.*, 2007). Without adequate treatment, these dyes can remain in the environment for a long time (Hao *et al.*, 2000).

To mitigate the effects wastewater pollution, various water treatment techniques are being used. Adsorption is regarded as efficient due to low cost, greater efficiency and effectiveness (Sohail et al., 2019; Bhatti *et al.*, 2018). The conventional techniques of water treatment like coagulation/flocculation, bed filtration, membrane filtration, precipitation, biodegradation and oxidation are unable to treat wastewater properly (Afroze & Sen, 2018; Ayad & El-Nasr, 2010). Due to design simplicity and flexibility, adsorption has been proven superior to various other techniques (Choudhary *et al.*, 2020; Lin *et al.*, 2014; Natarajan *et al.*, 2018). Recently, activated carbons have gained much attention for the adsorption of dyes and heavy metals. Activated carbon is one of the efficient adsorbents preferred for wastewater treatment and remediation due to its extended surface area, porous structure, high adsorptive capacity and high degree of surface reactivity (El Hammari *et al.,* 2022; Patra *et al.*, 2020; Belbachir *et al.,* 2013). For economic scalability in preparing activated carbons, cheap carbonaceous precursors such as lignocellulosic materials from agricultural waste are mostly preferred (Jawad *et al.*, 2020).

Several studies have exploited agricultural wastes (Sun *et al.*, 2021; Loulidi *et al.*, 2020; Jawad et al. 2020), composites (Liu *et al.*, 2019) and activated carbons (Wang *et al.*, 2020; Park *et al.*, 2019; Nizam *et al.*, 2021; Yao *et al.*, 2020) for the removal of water contaminants. Studies have been carried out on the adsorption of cationic dyes using Ziziphus species (Touzani *et al.*, 2022; Khan *et al.*, 2022). This Study investigates the adsorption capacity of activated carbon obtained from Ziziphus mauritania seed shell for the removal of MB, MO and RB dyes from mimicked dye-containing wastewater.

2. Materials and methods

2.1 Materials

The dyes used in this research are methylene blue (C.I. No. 52015, MW 319.85 g/mol, Λmax = 664 nm), methyl orange (C.I. No. 13025, MW 327.33 g/mol, Λmax = 487.10 nm) and rhodamine B (C.I. No. 45170, MW 479.02 g/mol, Λmax = 554.06). Drying of samples was carried out using a Hot air oven (Oven NYC 101), carbonization was carried out using a furnace (p – SLECTA), UV/Vis spectrophotometer (Lambda 35, Perkin Elmer) was used for measuring dye concentration, incubator shaker (Innova 4000, New Brunswick Scientific Co. Inc.) was used for the agitation of the adsorption mixture, FTIR spectrophotometer, Scanning electron microscope (SEM) were used for characterization.

2.2 Adsorbent preparation

The adsorbent was prepared as described by (Alabi *et al.*, 2020; Ibrahim and Umar, 2016). The ZM seed shells were washed thoroughly to remove any adhering dirt and left to dry under the sun. The dried material was pulverized and sieved using a 0.2 mm mesh sieve.

2.3 Preparation of activated carbons

The activated carbon of ZM was prepared by chemical activation with H_3PO_4 as per the procedure adopted by Pam *et al.,* 2022. Powdered ZM seed shell was mixed with the activating agent in a ratio 2:1 (activating agent to substrate) wt./wt., stirred intermittently for 30 min to make a slurry, and dried in an oven at 110 °C for 24 h. The sample was carbonized in a muffle furnace at 600 °C for 1 h. The resulting AC was washed several times with warm distilled water until the pH was neutral, then filtered and dried at 110 °C for 24 h.

2.4. Characterization of the substrates

The surface morphologies of the raw and carbonized substrates before and after the adsorption of dyes were determined using SEM. The Functional groups on the dye molecules and the surfaces of the adsorbents (before and after adsorption) were determined using an FTIR spectrophotometer.

2.5. Point of zero charge (pHpzc)

The point of zero charge of the adsorbents was determined by adding 0.1 g of the substrates different conical flasks containing 50 cm^3 of 0.1 M NaCl solutions of different pH (2, 4, 6, 8 and 10). The pH adjustment was carried out using either NaOH or HCl as appropriate. The containers were sealed and agitated on a mechanical shaker at ambient temperature for 4 h after which the final pH values were

measured. The difference between the initial and final pH were calculated and plotted against the initial pH. The intercept of the resulting curve at which ΔpH = 0 represents the point of zero charge (Ofudje *et al.*, 2015; Jawad *et al.*, 2021).

2.6. Moisture content

3 g of the sample was placed in a crucible of known weight and heated in the oven at 110°C. The samples were removed and re-weighed at time intervals of 10 minutes until constant weight was attained. The final weight was recorded and the moisture content was calculated using equation (1) (Ohimora *et al.* 2021):

$$Moisture\ content\ (\%) = \frac{W_2 - W_3}{W_2 - W_1} \times 100 \quad (1)$$

Where W_1 represents the weight of the empty crucible, W_2 and W_3 are the weights of crucibles containing moist activated carbon and dried activated carbon respectively.

2.7. Ash content

3 g of the sample was placed in a pre-weighed crucible and heated in a furnace at 700°C for 120 minutes. The crucible was allowed to cool down to room temperature and weighed. The Ash contents were calculated using equation (2) (Gaya *et al.*, 2016):

$$Ash\ content\ (\%) = \frac{W_3 - W_1}{W_2 - W_1} \times 100 \quad (2)$$

Where W_1 is the weight of the empty crucible, W_2 is the weight of the crucible containing the sample and W_3 is the weight of the crucible containing the ash.

2.8. Determination of Bulk Density

Bulk densities of d ZM and ZM-H_3PO_4 were determined using the method in Evwierhoma *et al.*, 2018 as follows: An empty graduated measuring cylinder was weighed then filled with a sufficient amount of the activated carbon with constant tapping up to the mark and weighed again. The bulk density was calculated using equation (3).

$$Bulk\ Density = \frac{W_c}{V_C} \quad (3)$$

Where W_c (g) is the weight of the dried activated carbon and V_c (cm^3) is the volume of the cylinder occupied by the activated carbon.

2.9. Batch adsorption experiment

1000 mg /dm^3 stock solutions of MB, MO and RB dyes were prepared. Lower concentrations were obtained by successive serial dilution. The adsorption capacities of ZM adsorbents were examined under

various conditions to determine the effects of contact time (10 – 120 min), adsorbent dose (0.1 – 1 g), initial dye concentration (10 – 100 mg/dm^3), pH of the medium (2 – 12), and temperature the adsorption process (303.15 – 333.15 K). Erlenmeyer flasks containing 100 ml of the dye solutions and the adsorbent were agitated in an incubator shaker. At pre-set time intervals, aliquots of the dye were withdrawn from the solutions and filtered. The filtrates were analysed using a UV/Vis spectrophotometer at the respective Λ_{max} of the dyes to determine the residual dye concentrations after adsorption (Shehu *et al.*, 2022).

3. Results and Discussion

3.1. Characterization

3.1.1. SEM

Figure 1 shows SEM images of ZM and its acid-activated derivative (ZM-H_3PO_4) before and after adsorption. The micrographs show evident pores of various sizes, ridges and cavities on the surface of the adsorbent, unlike the raw substrate which exhibited a smooth surface.

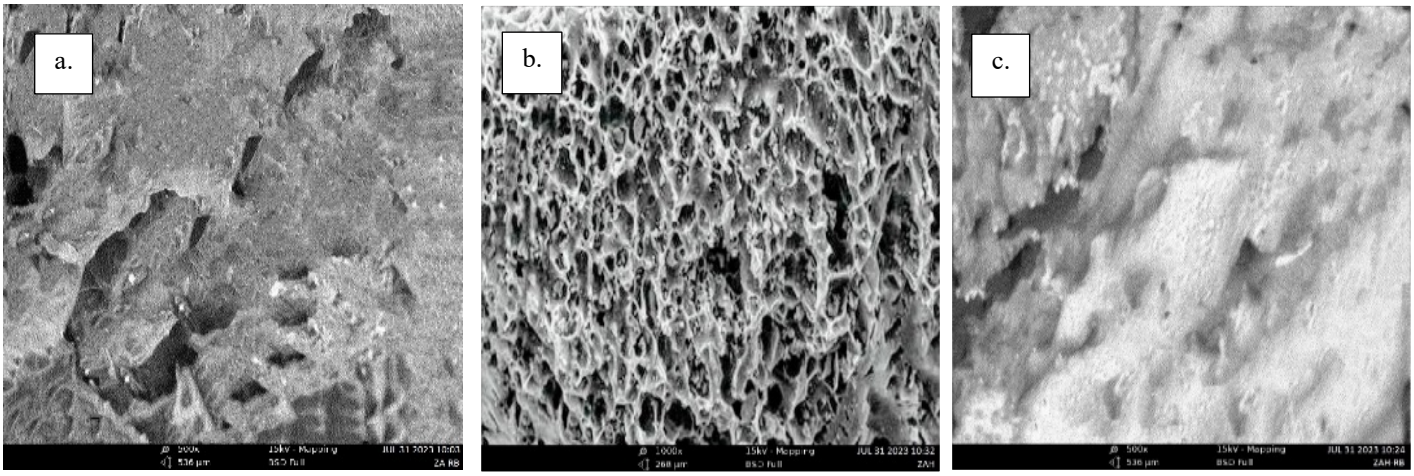

Figure 1. SEM Images of (a) ZM, (b) ZM-H_3PO_4 before Adsorption, (c) ZM-H_3PO_4 after Adsorption.

The activation as well as the pyrolysis might be the causes of the pores that were created on the surface of the activated carbon. It could also be concluded that the high porosity observed on ZM-H_3PO_4 is because, during the activation process, phosphoric acid acts as a catalyst which leads to the further incorporation of H_3PO_4 into the interior of the biomass structure, thereby enhancing the decomposition of the polymers (Habila *et al.*, 2014). After dye adsorption, the surfaces of the ZM-H_3PO_4 became less porous, and the cracks vanished, indicating effective loading of the dye molecules onto the adsorbent surface.

3.1.2. FTIR

The FTIR spectra of the biomass precursor ZM and its phosphoric acid-activated carbon ZM-H_3PO_4 before and after the adsorption of RB are presented in Figure 2. The spectra show a broad absorption

band at 3100 – 3500 cm^{-1} indicating hydroxyl group –OH stretch. The peak at 2950 cm^{-1} can be assigned to the alkane C─H stretch.

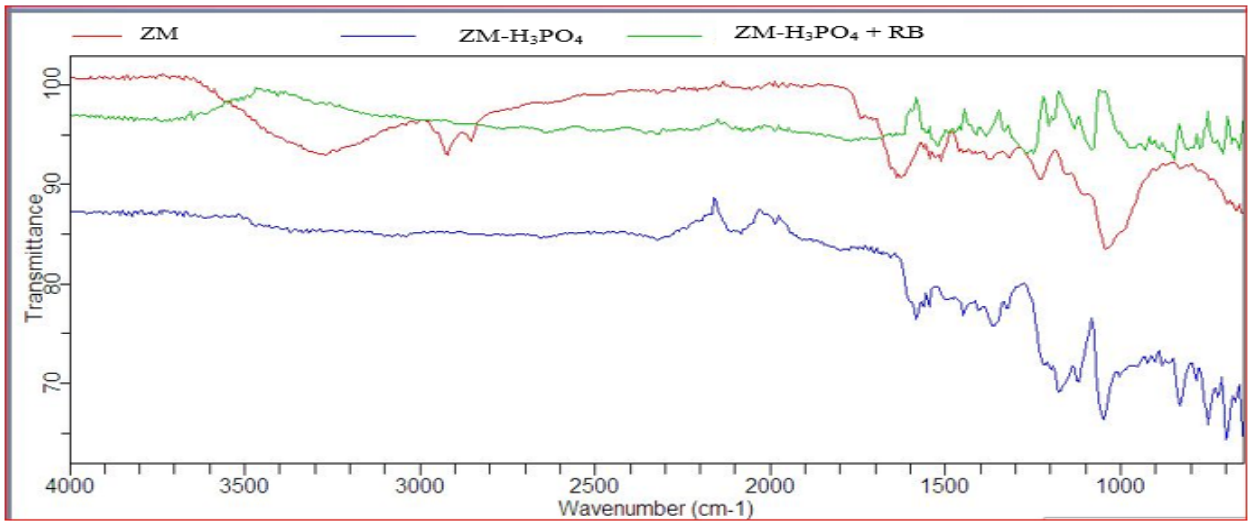

Figure 2. FTIR Spectra of ZM and ZM-H_3PO_4 before and after Adsorption of RB

The peak observed around 2100 can be attributed to alkyne C≡C stretch whereas bands at 1600 and 1650 cm^{-1} are due to conjugated alkene C=C stretch. The presence of bands around 1450 cm^{-1} signifies alkane C─H bending while the peak around 1350 cm^{-1} indicates O–H bending. The absorption bands located at 1050 to 1200 cm^{-1} are assigned to the stretching of C─O. After activation of the precursor by H_3PO_4, alterations in the observed peaks are evident. The bands corresponding to –OH and C─H stretching have been eliminated. The intensity of the alkene C=C stretching has reduced after activation and RB adsorption and the peaks at 1000 to 1500 cm^{-1} have shifted wave numbers indicating the cleavage of some weak bonds in the original compound.

3.2. Point of zero charge

Figure 3 shows the pH_{pzc} of the raw ZM and activated ZM-H_3PO_4 adsorbents. The point of zero charge increased from 6.3 to 7.6 after acid activation.

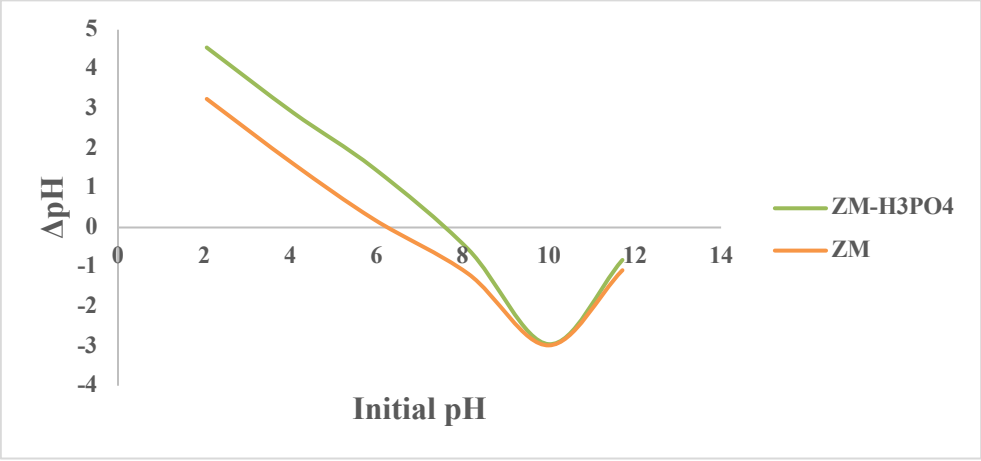

Figure 3. pH_{pzc} for ZM and ZM-H_3PO_4

Adsorbents with low pH_{pzc} have a high affinity to cationic molecules while those with high pH_{pzc} tend to bind more with anionic molecules (Ayuba *et al.*, 2022).

3.3. Proximate analysis and bulk density

Table 1 shows the Bulk densities, moisture and ash contents of ZM and ZM-H_3PO_4. The raw adsorbent shows a moisture content of 3.55% whereas the activated carbon, ZM-H_3PO_4, exhibited less moisture content of a value of 2.99%.

Table 1. Moisture and Ash Contents and Bulk densities of the Adsorbents.

S/N	Adsorbent	Moisture Content (%)	Ash Content (%)	Bulk Density (g/cm^3)
2	ZM	3.55	1.76	0.82
4	ZM-H_3PO_4	2.99	37.68	0.68

The moisture contents found in this study are far less than the value reported by Ohimor *et al.* (2021). The ash content increased from 1.76% for ZM to 37.68% after acid activation (ZM-H_3PO_4). The result of bulk density shows a minimal decrease from 0.82 g/cm^3 for ZM to 0.68 g/cm^3 for ZM-H_3PO_4. The bulk densities of the raw and acid-derived activated carbon are higher than those reported by Adebayo *et al.* (2020) who obtained 0.4408, 0.3316 and 0.3638 g/cm^3.

3.4. Effect of contact time

The influence of contact time on the removal of MB, MO and RB by ZM-H_3PO_4 is shown in Figure 4. The adsorbent has shown the highest affinity for RB with a removal quantity of 89.15 mg/g followed by MB then MO with removal quantities of 80.79 and 79.24 mg/g respectively.

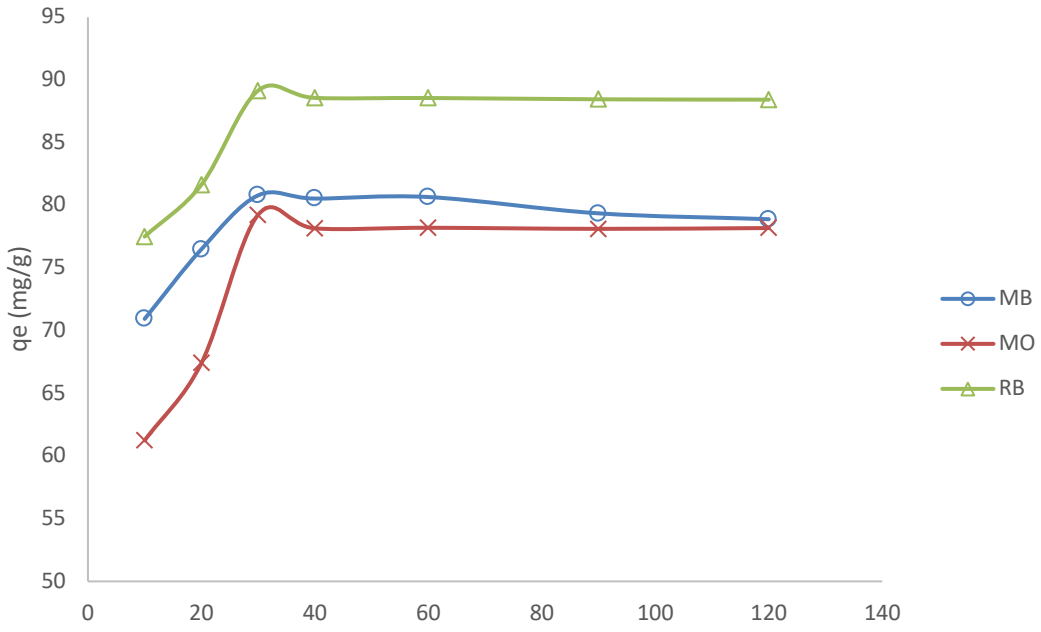

Figure 4. Effect of contact time on the adsorption of MB, MO and RB onto ZM-H_3PO_4

The adsorption rate increases steadily until it reaches equilibrium then it stops. This may be due to the availability of adsorption sites at the initial stage of the process which are later occupied as the adsorption proceeds. The adsorptions were nearly stable after 30 mins in all three dyes, this was considered the point of equilibrium. The findings here are similar to the work of Hamzezadeh *et al.* (2020).

3.5. Effect of adsorbent dosage

The effect of ZM-H_3PO_4 dosage on the adsorption of MB, MO and RB was analysed in Figure 5. The adsorption capacity for all the dyes decreased when the adsorbent loading is increased.

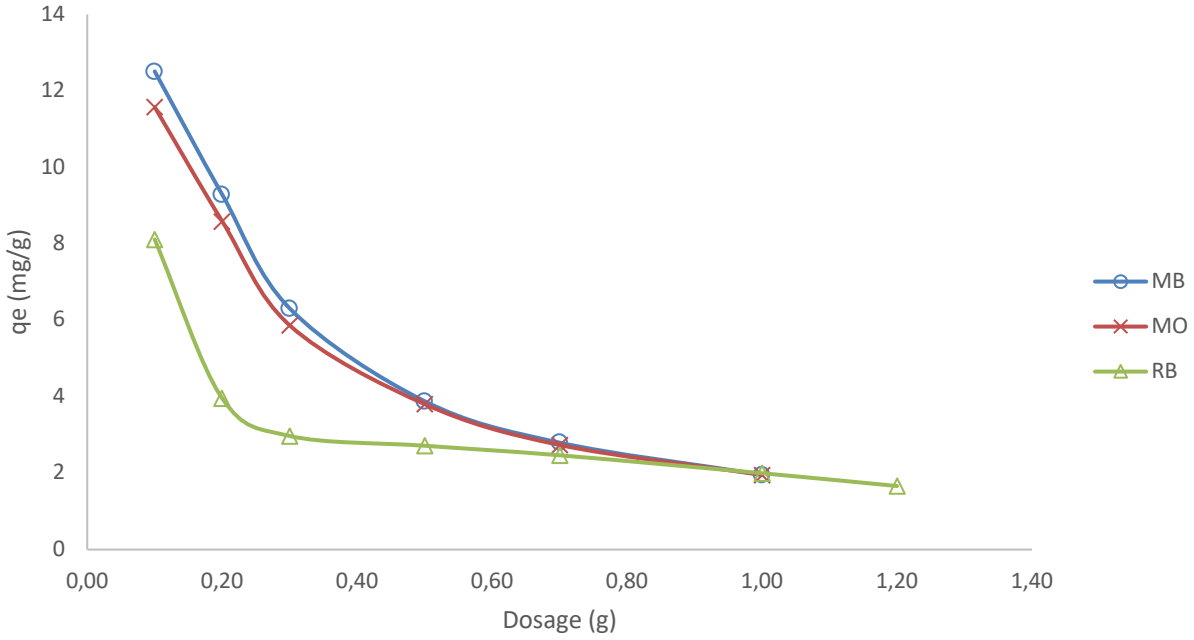

Figure 5. Effect of ZM-H_3PO_4 on the Removal of MB, MO and RB from Water

The highest adsorbed dye is MB followed by MO then RB with adsorption capacities of 12.51, 11.57 and 8.11 mg/g respectively. The removal capacity for RB declined to 1.66 mg/g. Those of MB and MO also followed the same trend where a decline of adsorption capacity to 1.95 mg/g was observed for both dyes when ZM-H_3PO_4 loading was increased from 0.1 to 1 g/100 cm^3. This might be due to the decrease in the available adsorption sites as a result of adsorbent aggregation when the adsorbent load is increased. This result is congruent with the findings of Lafi *et al.* (2018).

3.6. Effect of initial dye concentration

The variation in the removal of MB, MO and RB with change in initial concentration was analysed and depicted in Figure 6. According to the data presented, the removals of MB, MO and RB increased with an increase in their initial concentrations.

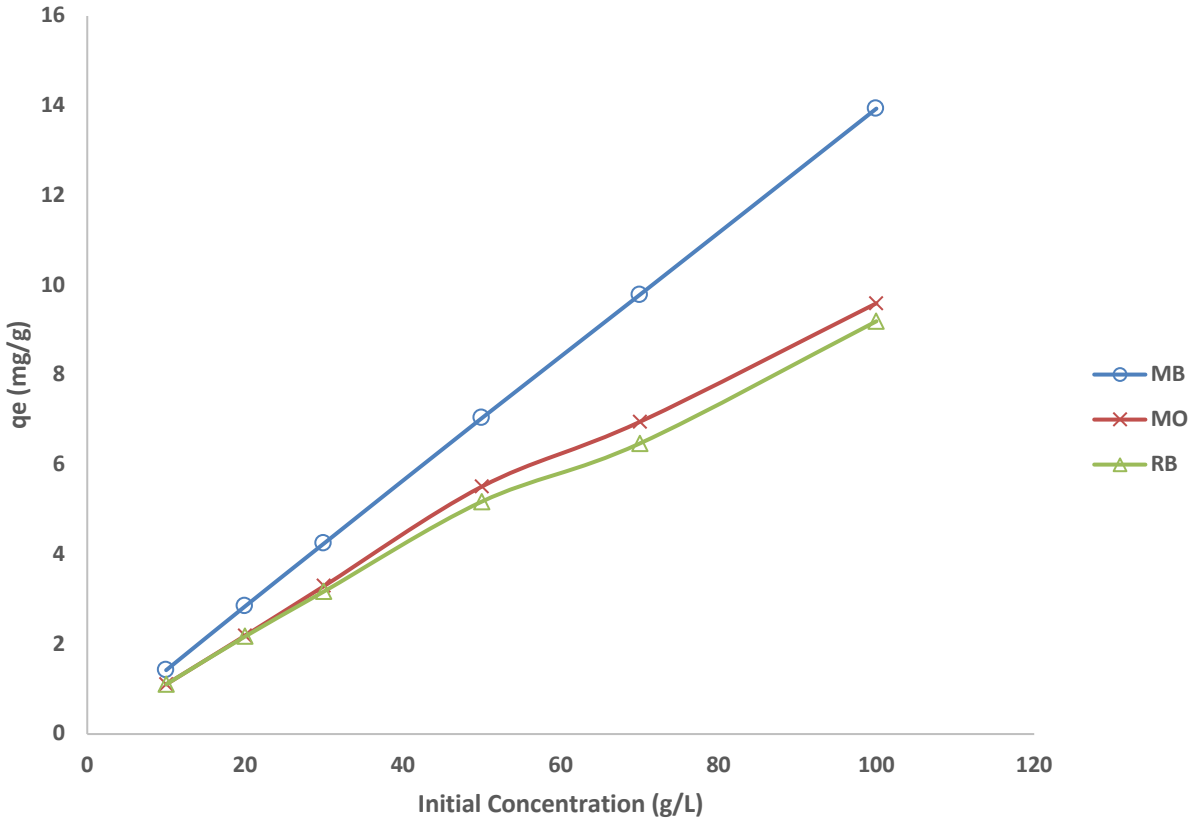

Figure 6. Effect of Initial Concentration on the Adsorption of MB, MO and RB by ZM-H_3PO_4

The rates of removal increase from 1.42 to 13.93 mg/g for MB, then from 1.10 to 9.59 mg/g for MO and from 1.10 to 9.19 mg/g for RB when the initial concentrations of the dyes increase from 10 to 100 mg/dm^3. The observed behaviour might be because the increase in the initial concentrations of the dyes causes an increase in its interaction with the adsorbent surface leading to greater adsorption. (Mohammadi *et al.*, 2011). Similar trends have been reported by Boudechiche *et al.* (2019) on the adsorption of BY28 and RB46 onto activated carbon derived from *Ziziphus lotus* stones at the initial concentration ranges of 80 to 250 mg/dm^3.

3.7. Effect of temperature

Figure 7 shows the variation of adsorption of MB, MO and RB with a change in temperature using ZM-H_3PO_4 as adsorbent. When the temperature increased from 303.15 to 333.15 K, the rates of removals of MB increased from 2.65 to 2.73 mg/g, the removal of MO also increased from 4.54 to 4.75 and in the same vein the adsorption of RB increased from 0.91 to 0.96 mg/g. This could be due to the accelerated mobility of MB, MO and RB or a decrease in the viscosity of the solution which increases the diffusion rate of the molecules in the pores of the adsorbent. Similar findings were reported in Das *et al.* (2018).

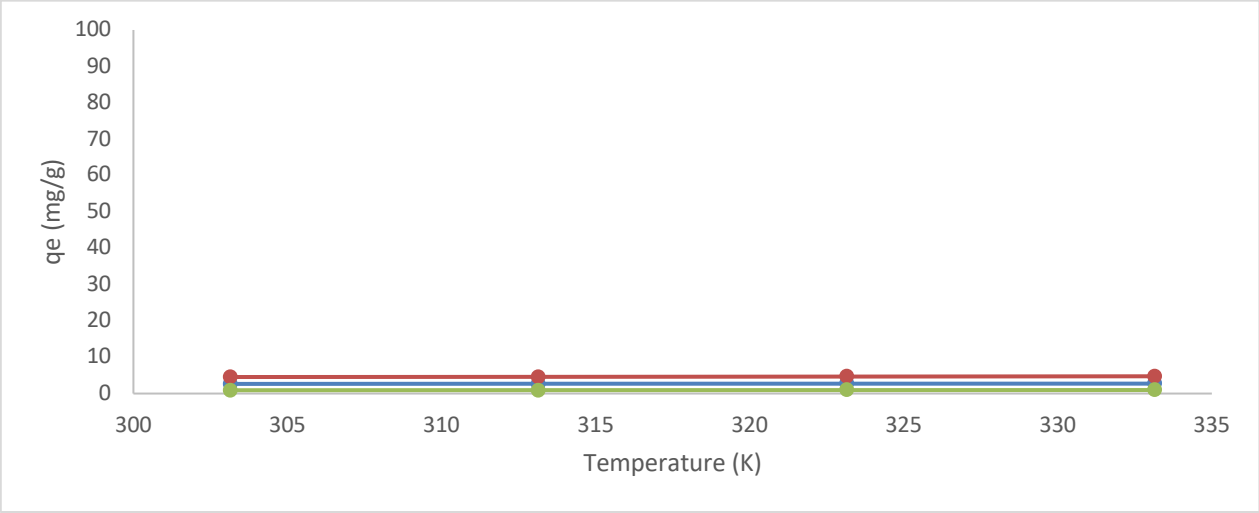

Figure 7. Influence of Temperature Change on the Removal of MB, MO and RB using ZM-H_3PO_4 Adsorbent

3.8. Effect of solution pH

The impact of pH on the removal of MB, MO and RB is described in Figure 8. The removals of MB and RB were observed to increase with the increase in pH with a marked increase above pH 8.

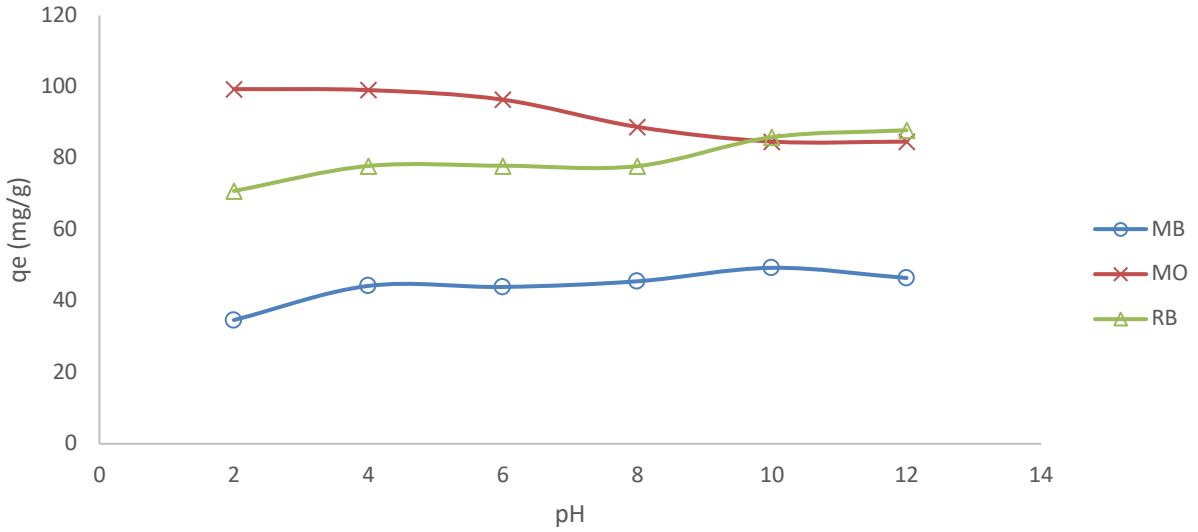

Figure 8. Effect of pH on the adsorption of MB, MO and RB onto ZM-H_3PO_4

Typically, the adsorption capacity of MB increased from 34.66 to 46.44 mg/g when the solution pH increased from 2 to 10. The adsorption of RB increased from 70.81 mg/g at pH 2 to 87.83 mg/g at pH 12. Meanwhile, the adsorption of MO decreases from 99.35 mg/g at pH 2 to 84.63 mg/g at pH 12. The low adsorption of MB and RB at low pH could be due to the competition for active adsorption sites between the cationic dye molecules and H^+ produced at acidic conditions. Meanwhile, this condition favours the accelerated removal of MO due to the electrostatic attraction between the anionic dye molecules and the protonated adsorbent surface. When the pH is raised above the pH_{pza} of ZM-H_3PO_4 which is 7.6, the adsorption of MO is lowered while that of MB and RB were increased markedly. This

might be because, at pH > pH_{pza}, the active groups on ZM-H_3PO_4 became deprotonated which renders the adsorbent surface negative (Yao *et al.*, 2020) hence attracting the cationic MB and RB and repels the anionic MO. The report here is congruent with the work of Vigneshwaran *et al.*, (2021).

3.9. Adsorption kinetics

The kinetic parameters for the adsorption of MB, MO and RB onto ZM-H_3PO_4 are shown in Table 2. The results show that the R^2 values of PSO (0.9996, 0.9990 and 0.9997) are higher than those obtained by PFO and Elovich models.

Table 2. Kinetic Parameters for the Adsorption of MB, MO and RB onto ZM-H_3PO_4

S/N	Kinetics Model	Parameters	Values		
			MB	MO	RB
1.	Pseudo-First Order	q_e (mgg^{-1})	68.0613	139.7977	94.5584
		K_1 (min^{-1})	0.1614	0.1607	0.1647
		R^2	0.9182	0.8415	0.8436
2.	Pseudo-Second Order	q_e (mgg^{-1})	79.3651	80.0000	89.2857
		K_2 ($gmg^{-1}min^{-1}$)	0.0794	0.0062	0.0112
		h ($mgg^{-1}min^{-1}$)	500.0000	39.5257	89.2857
		R^2	0.9996	0.9990	0.9997
3.	Elovich model	α ($mgg^{-1}min^{-1}$)	2594.5849	73.2729	2005.5599
		β (gmg^{-1})	0.1128	0.0642	0.0990
		R^2	0.9942	0.8952	0.9037

This indicates that PSO is the most appropriate model to describe the kinetics of adsorption of MB, MO and RB onto ZM-H_3PO_4. Additionally, the q_e values calculated from PSO (79.36, 80.00 and 89.29 mgg^{-1} for MB, MO and RB respectively) are more agreeable with the experimental values (80.79, 79.24 and 89.15 mgg^{-1}) than those suggested by PFO. This further corroborates the suitability of PSO to describe the kinetics of the adsorption process. By implication, the adsorption of MB, MO and RB is governed by the number of adsorption sites on ZM-H_3PO_4 rather than the dye concentrations and the process is chemisorption (Ling *et al.*, 2016). The result also reveals that the PSO adsorption rates for MB, MO and RB are 0.0794, 0.0062 and 0.0112 $gmg^{-1}min^{-1}$ respectively. This shows that the uptake of MB is the fastest followed by RB then MO. The results obtained here are similar to the report on the acid dyes onto modified Bentonite (Yan *et al.*, 2015).

3.10. Adsorption isotherms

Table 3 presents the Langmuir, Freundlich and Dubunin-Radushkevich model parameters for the adsorption of MB, MO and RB onto ZM-H_3PO_4. According to the results, the Freundlich model is more fitting for MB (R^2 = 0.9835) and RB (R^2 = 0.9797) adsorption data than Langmuir and Dubunin-Radushkevich.

Table 3. Isotherm Parameters for the adsorption of MB, MO and RB onto ZM-H_3PO_4

S/N	Isotherms	Parameters	Values		
			MB	MO	RB
1	Langmuir	q_{max} (mgg^{-1})	10.1420	9.7466	3.9541
		K_L (Lmg^{-1})	4.4818	1.2200	9.9960
		R^2	0.9804	0.9526	0.8650
		R_L	0.0083	0.0296	0.0038
2	Freundlich	K_F (Lmg^{-1})	8.4562	4.2704	3.1569
		n	1.9908	3.0675	3.0202
		R^2	0.9835	0.8484	0.9797
3	Dubinin-Radushkevich	q_s ($molg^{-1}$)	9.5630	5.9835	4.9412
		β (mol^2kJ^{-2})	0.0281	0.0246	0.0210
		E ($kJmol^{-1}$)	4.2182	4.5083	4.8795
		R^2	0.9014	0.7557	0.6581

It was observed that the K_F values are in the order MB > RB indicating superior adsorption capacity for MB than RB. For both MB and RB, the degree of non-linearity, n values are greater than one indicating that the adsorption is satisfactory. It can be deduced from the findings that MB and RB form multilayers over heterogeneous sites on the surface of ZM-H_3PO_4. It is also evident from the result that the adsorption of MO follows the Langmuir assumptions as revealed by the calculated R_L value (0.0296) which suggests favourable adsorption of MO as the value falls within the range of $0 < R_L < 1$. The R^2 value of 0.9526 indicates that the experimental data fits the Langmuir model. The calculated maximum adsorption capacity q_e (9.7466 mgg^{-1}) is comparable with the experimental value of 9.5985 mgg^{-1}. It can be concluded that MO is adsorbed by homogenous active sites to form a monolayer with no interaction between the dye molecules. The outcome of the Langmuir model fitting obtained corresponds with the report on the adsorption of crystal violet onto pyrophyllite with a calculated q_{max} of 9.58 mgg^{-1} (Miyah *et al.*, 2017; Miyah *et al.*, 2022) whereas the result of Freundlich fitting corresponds with the work of (Balkaya, 2019).

3.11. Thermodynamic studies

Table 4 shows the enthalpies, entropies and Gibb's free energies for the adsorption of MB, MO and RB onto ZM-H_3PO_4. The results show that all ΔG values are negative indicating the spontaneity of the adsorption of MB, MO and RB onto the adsorbent.

Table 4. Thermodynamic parameters for the adsorption of MB, MO and RB onto ZM-H_3PO_4

Adsorbent	Dye	ΔH (kJ/mol)	ΔS (kJ/mol. K)	−ΔG (kJ/mol)			
				303.15 K	313.15 K	323.15 K	333.15 K
ZM-H_3PO_4	MB	14.2618	0.0525	1.6620	2.1873	2.7125	3.2378
	MO	17.9807	0.0589	0.1106	0.4789	1.0683	1.6578
	RB	26.4078	0.0874	0.0941	0.9684	1.8426	2.7168

The values of enthalpy change are found to be positive in all the adsorption processes revealing that the processes are endothermic (Ech-chihbi *et al.*, 2016; Salim *et al.*, 2021). The ΔS values are also positive indicating the increase in randomness at the solid/liquid interface (Luo *et al.*, 2015). According to Bu *et al.* (2016), the cause of this could be attributed to water molecules being liberated as a result of molecular exchange between dye molecules and functional groups on the adsorbent surface, which led to greater irregularity at the solid/fluid boundary.

Conclusion

The phosphoric acid activation of the Ziziphus mauritania seed shell produced the activated carbon with marked porosity. In addition, the surface chemistry of the activated carbon reveals various functional groups that aided in the effective binding of the dye molecules. The optimization parameters; Contact time, adsorbent dosage and initial dye concentrations influence the adsorption efficiency of the activated carbon except for the temperature change which has a negligible effect. The maximum adsorption capacities of 80.79, 99.35 and 89.15 mg/g for MB, MO and RB were achieved at 30 minutes in neutral conditions. Therefore, it is concluded that ZM-H3PO4 can serve as a potential adsorbent that is effective in removing cationic and anionic dyes from wastewater.

References

Afroze S., Sen T. K., (2018) A Review on Heavy Metal Ions and Dye Adsorption from Water by Agricultural Solid Waste Adsorbents, *Water, Air, & Soil Pollution*, *229*(7), 225–275. https://doi.org/10.1007/s11270-018-3869-z

Alabi A. H., Oladele E. O., Adeleke A. J. O., Oni F. C., Olanrewaju C. A., (2020) Equilibrium, Kinetic and Thermodynamic Studies of Biosorption of Methylene Blue on Goethite Modified Baobab Fruit Pod (Adansonia Digitata L.), *Journal of Applied Science and Environmental Management,* 24(7), 1229– 1243.

Ayad M. M., El-Nasr A. A., (2010) Adsorption of Cationic Dye (Methylene Blue) from Water Using Polyaniline Nanotubes Base, *The Journal of Physical Chemistry C*, *114*(34), 14377–14383. https://doi.org/10.1021/jp103780w

Ayuba A. M. Sani M., (2022) Removal of Eriochrome Black T Dye from Aqueous Solution using Base Activated Typha Grass (Typha Latifolia) as an Adsorbent*, Bayero Journal of Pure and Applied Sciences*, 15(1), 95 –104.

Baban A., Yediler A., Ciliz, N. K., (2010) Integrated water management and CP implementation for wool and textile blend processes, *Clean*, 38 (1), 84–90.

Balkaya N., (2019) Biosorption of Dye from Aqueous Solutions by a Waste Lignocellulosic Material. In: Guneysu, S. (Ed.), Recycling and Reuse Approaches for Better Sustainability, *Springer International Publishing, Cham,* 277–295.

Belbachir C., Aouniti A., Khamri K., *et al.* (2013) Heavy metals (copper, zinc, iron and cadmium) in sediments and the small clam (Chamelea gallina) of the coastal area north-east of Morocco, *Journal of Chemical and Pharmaceutical Research*, 5 (12), 1307-1314

Bhatti H. N., Hayat J., Iqbal M., Noreen S., Nawaz S., (2018) Biocomposite application for the phosphate ions removal in aqueous medium, *Journal of Materials Research and Technology*, *7*(3), 300–307. https://doi.org/10.1016/j.jmrt.2017.08.010

Bu R., Chen F., Li J., Li W., Yang F., (2016) Adsorption Capability for Anionic Dyes on 2-Hydroxyethylammonium Acetate-Intercalated Layered Double Hydroxide, *Colloids and Surfaces A: Physicochemical and Engineering Aspects,* 511, 312– 319.

Choudhary M., Kumar R., Neogi S., (2020) Activated biochar derived from Opuntia ficus-indica for the efficient adsorption of malachite green dye, Cu^{+2} and Ni^{+2} from water, *Journal of Hazardous Materials*, *392*, 122441. https://doi.org/10.1016/j.jhazmat.2020.122441

Christie R. M. (2007), Environmental aspects of textile dyeing, *Elsevier*

Das T. R., Patra S., Madhuri R., Sharma P. K., (2018) Bismuth Oxide Decorated Graphene Oxide Nanocomposites Synthesized via Sonochemical Assisted Hydrothermal Method for Adsorption of Cationic Organic Dyes, *Journal of Colloids and Interface Science,* 509, 82-93.

Ech-chihbi E., Salim R., Oudda H., Elaatiaoui A., Rais Z., Oussaid A., El Hajjaji F., Hammouti B., Elmsellem H., Taleb M., (2016) Effect of some imidazopyridine compounds on carbon steel corrosion in hydrochloric acid solution, *Der Pharm Chem.,* 8(13), 214-230.

El Hammari L., Latifi S., Saoiabi S., Azzaoui K., *et al*. (2022) Toxic heavy metals removal from river water using a porous phospho-calcic hydroxyapatite, *Moroccan Journal of Chemistry* 10 (1), 62-72

Evwierhoma E. T., Madubiko O. D., Jaiyeola A., (2018) Preparation and Characterization of Activated Carbon from Bean Husk, *Nigerian Journal of technology*, 37(3), 674 – 678.

Gaya U. I., Otene E., Abdullah A., (2016) Adsorption of Aqueous Cd(II) and Pb(II) on Activated Carbon Nanopores Prepared by Chemical activation of *Hyphaene thebaica* Shell, *SpringerPlus*, 4, 458– 476.

Goscianska J., Ptaszkowska M., Pietrzak R., (2015) Equilibrium and Kinetic Studies of Chromotrope 2R Adsorption onto Ordered Mesoporous Carbons Modified with Lanthanum, *Chemical Engineering Journal*, 270, 140– 149.

Habila M. A., ALOthman Z. A., Ali R., Ghafar A. A., Hassouna M. S. E. D., (2014) Removal of Tartrazine Dye onto Mixed-Waste Activated Carbon: Kinetic and Thermodynamic Studies, *CLEAN Soil Air Water,* 42, 1824–1831.

Hamzezadeh A., Rashtbari Y., Afshin S., Morovati M., Vosoughi M., (2020) Application of Low-Cost Material for Adsorption of Dye from Aqueous Solution, *International Journal of Environmental Analytical Chemistry, 1–16*

Hao O. J., Kim H., Chang P. C., (2000) Decolorization of Wastewater, *Critical Reviews in Environmental Science and Technology,* 30, 449–505.

Hunger K., (2003) Industrial Dyes: Chemistry, Properties, Applications, *Wiley-VCH*, Weinheim

Ibrahim M. B., Umar A., (2016) Adsorption Thermodynamics of Some Basic Dyes Uptake from Aqueous Solution using *Albizia lebbeck* Shells, *ChemSearch Journal,* 7(1), 43 – 51.

Jawad A. H., Abdulhameed A. S., Mastuli M. S., (2020) Acid-Factionalized Biomass Material for Methylene Blue Dye Removal: A Comprehensive Adsorption and Mechanism Study, *Journal of Taibah University for Science,* 14(1), 305–313.

Jawad A. H., Saud Abdulhameed A., Wilson L. D., Syed-Hassan S. S. A., ALOthman Z. A., Rizwan Khan M., (2021) High Surface Area and Mesoporous Activated Carbon from KOH-Activated Dragon Fruit Peels for Methylene Blue Dye Adsorption: Optimization and Mechanism Study, *Chinese Journal of Chemical Engineering*, 32, 281–290.

Keharia H., Madamwar D., (2003) Bioremediation Concepts for Treatment of Dye Containing Wastewater: a Review, *Indian Journal of Experimental Biology,* 41(9), 1068–1075.

Khan T. A., Nouman M. D., Dua D. Khan S. A., Alharthi S. S., (2022) Adsorptive Scavenging of Cationic Dyes from Aquatic Phase by H_3PO_4 Activated Indian Jujube (Ziziphus mauritiana) Seeds based Activated Carbon: Isotherm, Kinetics, and Thermodynamic Study, *Journal of Saudi Chemical Society,* 26(2), 101417–101433.

Lafi R., Montasser I., Hafiane A., (2018) Adsorption of Congo Red Dye from Aqueous Solutions by Prepared Activated Carbon with Oxygen-Containing Functional Groups and its Regeneration, *Adsorption Science and Technology,* 37(1-2), 160–181.

Lin C. H., Gung C. H., Sun J. J., Suen S. Y., (2014) Preparation of polyethersulfone/plant-waste-particles mixed matrix membranes for adsorptive removal of cationic dyes from water, *Journal of Membrane Science*, *471*, 285–298. https://doi.org/10.1016/j.memsci.2014.08.003

Ling F., Fang L., Lu Y., Gao J., Wu F., Zhou M., Hu B., (2016) A Novel Co-Fe Layered Double Hydroxides Adsorbent: High Adsorption Amount for Methyl Orange Dye and Fast Removal of Cr (VI), *Microporous and Mesoporous Materials,* 234, 230–238.

Liu X., Tian J., Li Y., Sun N., Mi S., Xie Y., Chen Z., (2019) Enhanced Dyes Adsorption from Wastewater via Fe3O4 Nanoparticles Functionalized Activated Carbon, *Journal Hazard Materials,* 373, 397–407.

Loulidi I., Boukhlifi F., Ouchabi M., Amar A., Jabri M., Kali A., Aziz F., (2020) Adsorption of Crystal Violet onto an Agricultural Waste Residue: Kinetics, Isotherm, Thermodynamics, and Mechanism of Adsorption, *The Scientific World Journal,* 2020, 5873521–5873530.

Luo Z., Gao M., Ye Y., Yang S., (2015) Modification of Reduced-charge Montmorillonites by a Series of Gemini Surfactants: Characterization and Application in Methyl Orange Removal, *Applied Surface Science,* 324, 807–816.

Miyah Y., Lahrichi A., Idrissi M., Anis K., Kachkoul R., Idrissi N., Lairini S., Nenov V., Zerrouq F., (2017) Removal of Cationic Dye ‘‘‘Crystal Violet’” in Aqueous Solution by the Local Clay, *Journal of Materials and Environmental Science,* 8, 3570–3582.

Miyah Y., Benjelloun M., Salim R., Nahali L., Mejbar F., Lahrichi A., Iaich S., Zerrouq F., (2022) Experimental and DFT theoretical study for understanding the adsorption mechanism of toxic dye onto innovative material Fb-HAp based on fishbone powder, *Journal of Molecular Liquids*, 362,119739.

Mohammadi N., Khani H., Gupta V. K. Amereh E., Agarwal S., (2011) Adsorption Process of Methyl Orange Dye onto Mesoporous Carbon Material-Kinetic and Thermodynamic Studies, *Journal of Colloid and Interface Sciences*, 362, 457–462.

Natarajan S., Bajaj H. C., Tayade, R. J., (2018) Recent advances based on the synergetic effect of adsorption for removal of dyes from waste water using photocatalytic process, *Journal of Environmental Sciences*, 65, 201–222. https://doi.org/10.1016/j.jes.2017.03.011

Nizam N. U. M., Hanafiah M. M., Mahmoudi E., Halim A. A., Mohammad A. W., (2021) The Removal of Anionic and Cationic Dyes from an Aqueous Solution using Biomass-Based Activated Carbon, *Scientific Reports*, 11(1), 8623–8640.

Ofudje E. A, Akiode O. K, Oladipo G. O, Adedapo A. E, Adebayo L O, Awotula A. O., (2015) Application of Raw and Alkaline-Modified Coconut Shaft as a Biosorbent for Pb^{2+} Removal, *BioResources*, 10 (2), 3462–3480.

Ohimora E. O., Temisaa D. O., Ononiwub P. I., (2021) Production of Activated Carbon from Carbonaceous Agricultural Waste Material: Coconut Fibres, *Nigerian Journal of Technology*, 40(1), 19–24.

Pam A. A., Abdullah A. H., Tan Y. P., Zainal Z., (2022) Physicochemical Properties of Porous Activated Carbon Prepared from Palm Kernel Shell Through a low-cost Activation Protocol, *South African Journal of Science,* 119(9), 13497–13504

Park J. H., Wang J. J., Meng Y., Wei Z., DeLaune R. D., Seo, D. C., (2019) Adsorption/Desorption Behavior of Cationic and Anionic Dyes by Biochars Prepared at Normal and High Pyrolysis Temperatures, *Colloids and Surfaces A: Physicochemical and Engineering Aspects,* 572, 274–282.

Patra C., Gupta R., Bedadeep D., Narayanasamy S., (2020) Surface Treated Acid-Activated Carbon for Adsorption of Anionic Azo Dyes from Single and Binary Adsorptive Systems: A Detail Insight, *Environmental Pollution, 115102–115120.*

Ramsay R. R., Dunford C., Gillman C. K., (2007) Methylene Blue and Serotonin Toxicity: Inhibition of Monoamine Oxidase A (MAO A) Confirms a Theoretical Prediction, *British Journal of Pharmacology*, 152 (6), 946–951. 10.1038/sj.bjp.0707430

Salim R., Nahlé A., El-Hajjaji F., Ech-chihbi E., Benhiba F., El Kalai F., Benchat N., Oudda H., Guenbour A., Taleb M., Warad I., (2021) Experimental, density functional theory, and dynamic molecular studies of imidazopyridine derivatives as corrosion inhibitors for mild steel in hydrochloric acid, *Surface Engineering and Applied Electrochemistry*, 57(2), 233-254.

Shehu A., Ibrahim, M. B., (2022) Adsorption and Desorption Studies of Dyes onto Pyrolysed Chemically Activated Shea Butter (Vitellaria paradoxa), *Bayero Journal of Pure and Applied Sciences*, 13(1), 283 – 290.

Sohail I., Bhatti I. A., Ashar A., Sarim F. M., Mohsin M., Naveed R., Yasir M., Iqbal M., Nazir A., (2020) Polyamidoamine (PAMAM) dendrimers synthesis, characterization and adsorptive removal of nickel ions from aqueous solution, *Journal of Materials Research and Technology*, *9*(1), 498–506. https://doi.org/10.1016/j.jmrt.2019.10.079

Sun Z., Qu K., Cheng Y., You Y., Huang Z., Umar A., Ibrahim Y. S. A., Algadi H., Castañeda L., Colorado H. A., Guo, Z., (2021) Corncob-derived Activated Carbon for Efficient Adsorption Dye in Sewage, *ES Food and Agroforestry,* 4, 61–74.

Suteu D., Zaharia C., Malutan T., (2011) Biosorbents Based on Lignin Used in Biosorption Processes from Wastewater Treatment (chapter 7). In: Lignin: Properties and Applications in Biotechnology and Bioenergy, Ryan J. Paterson (Ed.), *Nova Science Publishers*, 27, ISBN 978-1-61122-907-3, New York, U.S.A.

Touzani I., Fikri-Benbrahim K., Ahlafi H., Ihssane B., Boudouch O., (2022) Characterization of *Ziziphus lotus'* Activated Carbon and Evaluation of Its Adsorption Potential, *Journal of Environmental and Public Health,* 2022, 1 – 12

Vigneshwaran S., Sirajudheen P., Karthikeyan P., Meenakshi S., (2021) Fabrication of Sulfur-Doped Biochar Derived from Tapioca Peel Waste with Superior Adsorption Performance for the Removal of Malachite Green and Rhodamine B dyes, *Surfaces and Interfaces,* 23, 100920–100930.

Wang H., Li Z., Yahyaoui S., Hanafy H., Seliem M. K., Bonilla-Petriciolet A., Luiz Dotto G., Sellaoui L., Li, Q., (2020) Effective Adsorption of Dyes on an Activated Carbon Prepared from Carboxymethyl Cellulose: Experiments, Characterization and Advanced Modelling, *Chemical Engineering Journal,* 417, 128116–128127.

Yan L., Qin L., Yu H., Li S., Shan R., Du B., (2015) Adsorption of Acid Dyes from Aqueous Solution by CTMAB Modified Bentonite: Kinetic and Isotherm Modeling, *Journal of Molecular Liquids,* 211, 1074 –1081.

Yao X., Ji L., Guo J., Ge S., Lu W., Chen Y., Cai L., Wang L., Song W., (2020) An Abundant Porous Biochar Material Derived from Wakame (Undaria pinnatifda) with High Adsorption Performance for Three Organic Dyes, *Bioresource Technology,* 318, 124082–124091.